Automation in Construction 145 (2023) 104639

Contents lists available at ScienceDirect

Automation in Construction

journal homepage: www.elsevier.com/locate/autcon

Monitoring Precast Structures During Transportation Using A Portable Sensing System

Sadia Umer Khayam, Jongbin Won, Junsik Shin, Junyoung Park, Jong-Woong Park *

Department of Civil and Environmental Engineering, Urban Design and Studies, Chung-Ang University, Seoul 06974, Republic of Korea

ARTICLE INFO

Keywords:
Precast delivery
Supply chain monitoring
Structural health monitoring
Portable sensor
Strain sensing

ABSTRACT

During the delivery process, precast concrete structures (PCS) undergo drastic changes in strain response that could induce damage resulting from the lifting process or shocks during delivery. However, the continuous logging of vibration and strain measurement during the delivery of a PCS remains limited because of difficulties related to sensor installation and condition assessment. This paper presents (1) a multimetric portable sensing system that simultaneously measures strain and acceleration, and (2) a safety assessment strategy that adjusts the offset of the initial strain measurement and calculates the absolute strain response for assessing the safety of PCS during the delivery process. The experimental validation was performed during the 80-min delivery process of a 12-m-long PCS. The acceleration, tilts and strain of the structure were measured during its delivery, and the measured data were processed and analyzed to conduct a safety assessment.

1. Introduction

Precast concrete structures (PCS) are manufactured in controlled factory environments and are widely used in construction projects to reduce workforce dependency and construction time [1–3]. Quality control is efficient for the PCS as concrete mix curing and stability are carried out under a controlled environment [4]. The handling of such PCS warrants careful inspection and monitoring to ensure its quality and safe delivery to the installation site [5]. If a PCS is not handled appropriately, it may experience failures. In the past, PCS unit failures have been encountered during their lifting by using clamps and choked hitched chains [6]. In one such case, a PCS collapsed because of a crack in it, as mentioned in a cross-safety report published in the United Kingdom [7]. Generally, PCS failures during lifting are caused by weak cable joints, clamp failures, or cracks in the PCS. Furthermore, extensive research has been conducted on precast girders to identify the causes of their failure, including tilts and support conditions during lifting and delivery. Stratford and Burgoyne considered hanging beams supported by bearings during delivery as the most critical support condition [8,9]. Moreover, they computed beam tilt angle and the corresponding additional stress generated during lifting [10]. Fuente et al. [11] in their case study on lifting failures, concluded that despite implementation of several codes and guidelines, the lateral instability of girders induces cracks and high levels of deflection during lifting. They recommended the use of numerical simulation to evaluate the risks associated with the lateral instability of PCS. Wif et al. [12] evaluated the lifting strains of a steel-reinforced deck panel. They found that the maximum strain at the center of the panel crossed the limiting crack strain, which necessitates the monitoring of lifting conditions, but they did not address the safety of structures during lifting. Chris et al. [13] monitored and tested 28-m-long precast bridge decks to examine diverse lifting scenarios. The maximum tensile strain of 72 με was observed at the top of the deck panels during lifting, while the strain decreased when the decks were placed on supports. One of the reasons for the high strains encountered during lifting was the tightening of tie-downs (lifting straps). This highlights the importance of monitoring strain values during PCS delivery. The drawback of the aforementioned research, was the use of a heavy setup to be carried by truck during transportation, further the data was processed with initial zero strains instead of absolute strain which implies impracticality of work. Laszlo et al. [14] suggested that lifting points should be moved inward toward the center of a PCS from the extreme ends to avoid crack formation during the moving process. According to the literature [14], the strains due to lifting can be minimized by adjusting the lifting position. Holden et al. [15] observed the lifting strains of a 12-m-long bridge deck panel, in addition to conducting a lab-scale experiment, the research contains development of a 3D model by using the finite element (FE) numerical method to obtain the strains and stresses of the structure for validation. Their results

* Corresponding author.
E-mail address: jongwoong@cau.ac.kr (J.-W. Park).

https://doi.org/10.1016/j.autcon.2022.104639
Received 26 May 2022; Received in revised form 14 October 2022; Accepted 27 October 2022
Available online 16 November 2022

indicated that four-point lifting from the underside was preferable for reducing strains to almost zero in order to avoid crack propagation. Accordingly, unexpected strain responses can be reduced by analyzing the structural behavior of a PCS in advance and adjusting the lifting points. Unfortunately, these studies do not describe how to compute absolute strain. In addition, monitoring the stresses induced in a structure not only during lifting but also throughout the delivery process is critical to obtain information about the extent of damage to a structure. Arabi et al. observed and monitored the transportation of sign-support (truss) structures and performed fatigue analysis to predict the damage caused by road-induced excitations [16]. Moreover, to ensure human and asset safety, adequate planning before commencement of the delivery process is crucial for avoiding failure [17]. Different guidelines, for instance, "A Guide to Managing Risk in Construction," highlight the rules and methodologies relevant to the transportation of PCS [9,18]. However, these guidelines are limited to the design, manufacture, transportation, and storage of PCS, and they do not address the prevention of risks arising from uncertainties during construction and delivery. Even preventive methods that can reduce strain during lifting have been suggested in the above-referenced studies, the safety of a PCS cannot be guaranteed because of unforeseen events that might occur during the 'actual PCS transportation process.

Although lifting and monitoring techniques have been explored over the years, only a few monitoring applications have been developed thus far [19–22]. Tong et al. [23] presented a case study on the lifting of a building for seismic retrofitting. Their monitoring system consisted of wired sensors installed on hydraulic jacks to provide member displacement data to a computer. Furthermore, several researchers have attempted to automate the construction and monitoring process [24–26]. Nevertheless, research on the implementation of system automation during the lifting and delivery stages of PCS is limited. Goggins et al. [27] monitored a precast slab by using vibrating wire strain gauges embedded in the slab. Their data acquisition system consisted of data loggers, a vibrating wire interface, and multiplexers. The main disadvantage of this system was its high-power consumption. Chunli et al. [28] monitored the lifting of a multi-story beam grillage steel corridor, including the resulting stress and deflection. Their monitoring method involved the use of laptops, displacement meters, magnetic stands, and drawbars. The monitored results were compared against simulation data. The results obtained using the two systems were mutually consistent, indicating the applicability of their scheme. However, the installation of their system was a cumbersome and time-consuming process. Furthermore, battery life is a critical concern in the transportation of PCS to distant locations.

Although wired sensing is a common practice, it has a few limitations in the monitoring of airlift conditions because the data logger attached to the sensor must be lifted, which can cause power failure. Such a power failure leads to inadequate power supply in the continuous monitoring of PCS. Additionally, the process of attaching wires to the data acquisition system during transportation is incommodious. Any negligence can cause fluctuations in the measurements obtained using wired sensors or easily damage the wired links.

With advances in microcontroller unit (MCU) and sensing technologies, wired sensors are being replaced with portable sensing systems [29–32] in which the MCU, analog-to-digital converter (ADC), and battery are embedded. The AX-3D and Waspmote sensor platforms use an ADC resolution of 16 bits, whereas a higher resolution is required for PCS monitoring [33,34]. The NARADA sensing platform, developed at University of Michigan [35], is composed of a base station personal computer (PC) and a power supply unit, which is undesirable for observing PCS delivery. A sophisticated sensor platform Xnode with a high transmission rate was developed at University of Illinois [36]. Owing to the advantages of Xnode, it has been used as a host platform or to validate modified and advanced sensors [37,38]. Xnode offers multimetric data acquisition, but it does require a base station PC [37]. However, for the transportation and delivery of PCS, a high-fidelity sensor must be employed for behavior monitoring without the need for a base station PC.

Further, the behavior of PCS during lifting is unpredictable owing to changes in tilts. This suggests the need for a multichannel tilt-measurement sensor [10]. In recent years, multimetric sensing strategies for structural health monitoring have attracted attention [39–41]. Sarwar et al. [39] used a multimetric system to realize long-term wireless sensor operation by integrating a multimetric event-driven system (EDS) and Xnode, but its applicability was limited because of its event-driven nature. Fu et al. [37] developed a sensing platform with a power consumption of 280 mA and data processing of 176 mA per unit time. Nevertheless, the requirement of a PC for data acquisition renders the system ineffective for PCS monitoring. Since PCS monitoring demands efficient battery power consumption without the need of radio transmission, therefore, a portable sensing board is needed. Inspired by previous research, Won et al. [42] recently developed a multimetric sensing board by combining a high-resolution accelerometer and strain sensor with Xnode as the host platform. The developed sensor system has strong processing capabilities, low power consumption, and it does not require a base station PC. Won et al. [42] successfully conducted the experimental validation by measuring strain and acceleration at 100 Hz. However, more efficient data processing platform was required.

In addition to the problems associated with sensing, identification of the actual strain during resting and lifting is critical for maintaining the quality of PCS. Laszlo et al. [14] and Holden et al. [15] studied PCS field data under the lifting and resting conditions. However, they failed to determine the absolute strain, which makes system validation an impractical task. Therefore, there is a need for a method to determine absolute strains in order to monitor the lifting and resting conditions.

In this study, the deficiencies in the established practices are addressed through the development of a precast delivery monitoring system (PDMS) to monitor the delivery stages of PCS. The system developed herein is characterized by ease of attachment, efficient battery power supply, and high-resolution multimetric monitoring; in addition, an efficient safety assessment strategy is introduced. First,a multimetric, low-power-consumption sensor system was developed for real-time data acquisition. The developed PDMS sensor system can simultaneously measure three-axis acceleration and three-channel strains, perform downsampling and finite impulse response (FIR) filtering, and record data in real time. Second, the aforementioned safety assessment strategy that incorporates FE analysis is implemented to remove offsets in the strain measured during the entire PCS delivery process. The FE analysis aims to determine the strain gauge positions at which the strain is zero during the lifting stage. The strain gauges of the developed sensor are installed at the zero-strain locations on the PCS. The general strategy of precast monitoring is validated by conducting an experiment in which the delivery of a 12-m-long PCS is monitored using the PDMS. The obtained strain measurements are adjusted in the lifting stage. The level of strain is analyzed subsequently to determine the condition of the PCS. FE analysis is performed to reveal the reason for uneven strain distribution throughout the PCS. To ensure PCS safety, the support conditions are analyzed to achieve the minimum resting strain, and the results indicate the importance of contact condition, number of supports, and boundary conditions.

2. Proposed sensing system

In this section, the development process of the proposed PDMS that can monitor acceleration and strains is described. The PDMS is a portable system that can be easily installed on various types of PCS. It offers real-time processing, including data acquisition. Further, the PDMS performs safety evaluation to prevent material damage for ensuring secure PCS delivery, thereby avoiding lifting failures and onsite injuries. A 12-m-long PCS is selected to investigate the applicability of the developed system for validation.

2.1. PDMS (precast delivery monitoring system)

This study proposes a portable wireless sensing system consisting of a MCU, ADC, accelerometer, three channel strain gauge and a SD card for real-time continuous data storage as shown in Fig. 1. The developed PDMS is capable of sensing multimetric measurements, such as acceleration and strain, and saving data in real time owing to the rich computational resources of the Teensy 4.1 MCU used herein. Unlike traditional MCUs, Teensy 4.1 has a clock speed of 600 MHz, which can be varied dynamically without causing any noise issues. Additionally, the hardware consists of 8 MB of pseudo-static random-access memory (PSRAM) and 1 MB of built-in RAM for ample data storage, which facilitates real-time measurement and logging. The ADC in the PDMS offers eight differential inputs, of which three channels each were earmarked for acceleration and strain measurement, and two channels were open for analog sensing peripherals such as temperature and humidity sensors. Acceleration data was acquired using a high-sensitivity ADXL354 accelerometer with a low noise density of $22.5\mu g/\sqrt{Hz}$ and sensing range of ±2 g. Furthermore, strain sensing was performed using the embedded Wheatstone bridge circuit.

The enclosure and the printed circuit board (PCB) of the PDMS are depicted Fig. 1b and Fig. 1c, respectively.

To achieve constant monitoring of the PCS during its lifting and transportation, the developed system was required to save six-channel data in real time. The developed PDMS started performing measurements when the power was turned on using a switch and records acceleration and strain values at a predefined sampling frequency of 1000 Hz. The raw measurements were low-pass-filtered using a FIR filter and down sampled by 1/10 to achieve a sampling rate of 100 Hz. The MCU firmware was developed using the Arduino integrated development environment (IDE), and the code for storing the data in real time was based on the SdFat library [43].

2.2. Accuracy of the PDMS

The developed PDMS was tested to assess signal measurement noise. The noise test was performed over 200 s in a vibration-free environment (Fig. 2). For strain testing, a 120-Ω strain gauge (PL-60-11-3LJC-F) was connected to the PDMS. The root mean squared error (RMSE) of the measured acceleration was 0.12 mg in the ±2 g sensing range, and it was close to the specification of ADXL354, which has an RMSE of 0.11 mg over a 25 Hz bandwidth. The strain measurement was excited by a voltage of 3.3 V, and the calibration factor was 48,287 με /V. The RMSE of the measured strain was 1.526 με over a measurement range of

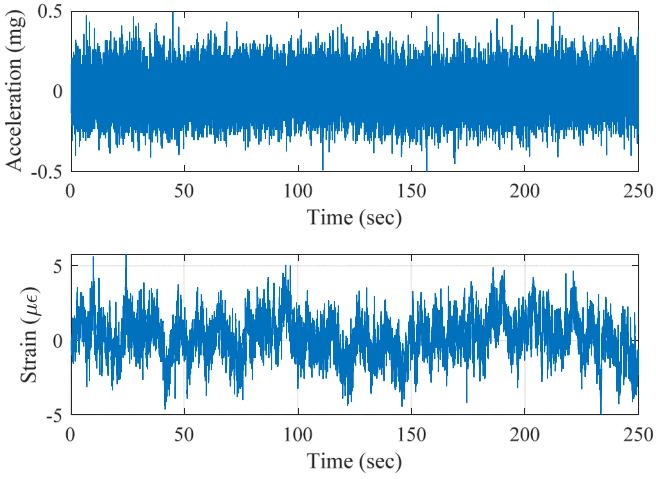

Fig. 2. Measured strain and acceleration noise of PDMS.

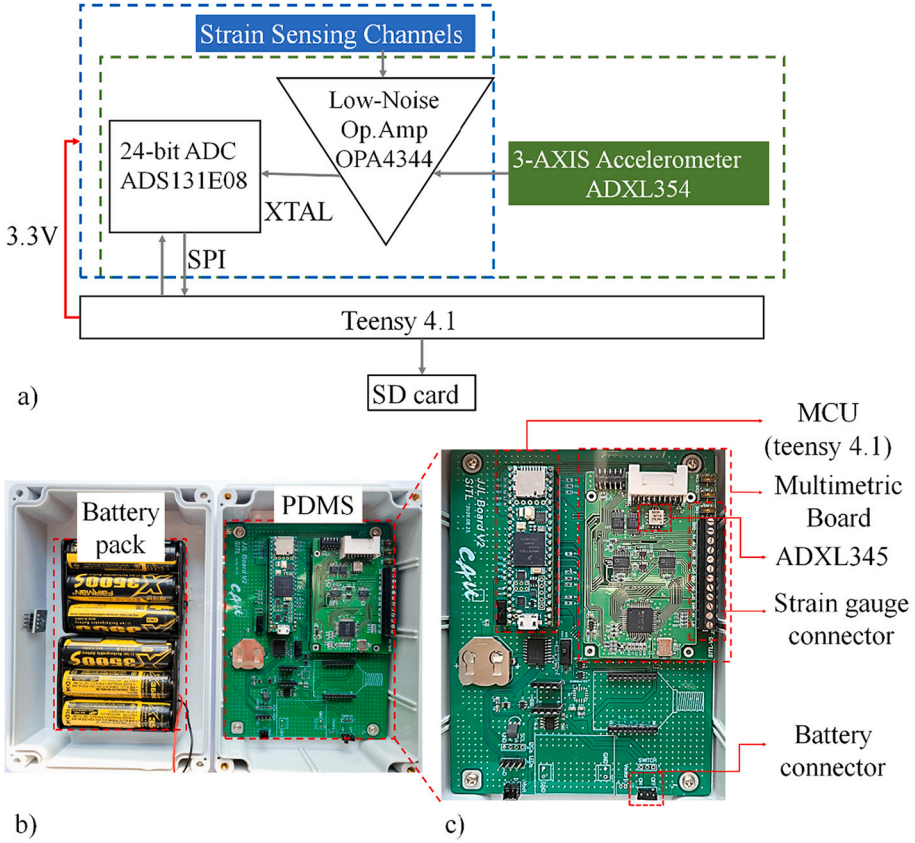

Fig. 1. Developed PDMS: a) Schematic diagram of hardware configuration, b) enclosure, and c) realized PCB.

±38,000 με.

2.3. Power consumption analysis of PDMS

To evaluate the performance of the PDMS, a power consumption analysis was performed. Table 1 presents the current consumption of the integrated system.

The current consumption of the sensor board is 26.518 mA, while the MCU consumes 100 mA, and three active strain gauges require 39 mA of current. The overall current consumption of the PDMS is 165.5 mA. A total of six 18,650 lithium-ion rechargeable batteries were deployed to ensure a battery capacity of up to 21,000 mAh. The battery life of the PDMS in terms of continuous operation hours was computed using Eq. (1) [44]:

$$Batt\_Life = \frac{Capacity}{I} \times 0.8 \tag{1}$$

where *Batt_Life* represents the battery life in hours, and *I* denotes the current consumption of the PDMS. The multiplication factor of 0.8 compensates for the effects of environmental and material conditions on battery life. The computed battery life of the PDMS is 4.2 days, which is sufficient for monitoring PCS in transit.

2.4. Safety assessment strategy

The existing safety reports emphasize the need to develop a delivery monitoring system that can ensure adequate safety during PCS delivery. The developed PDMS aids in the safety assessment of PCS by highlighting the threshold values of possible crack-inducing factors. The general working principle of the PDMS for safety assessment is illustrated in a flowchart in Fig. 3. The mentioned safety steps are applicable to all prefab structures that undergo the ground resting (GR), airlifting (AL), truck resting (TR), and transportation stages. The steps implemented for safety evaluation are described as follows.

Step1: Preprocessing (planning)

Before sensor installation, FE analysis should be carried out to determine the optimal sensor location and set the cracking limit for the structure. Strain can be measured at a location where it can provide reference value for offset adjustment. Since strain measurements only indicates the change in strain from the time at which the strain gauges are installed, it is extremely difficult to estimate the absolute strain and identify the actual stress acting on the structure. This study proposes offset adjustment of strain measurements by measuring strains at lifting stage, where the strain becomes zero. To achieve minimum strains, the strain measurement location should be determined carefully through FE analysis, and locations at which the strain becomes zero in the lifting stage should be identified.

Table 1
Current consumption of PDMS.

Device	Current Consumption
Sensor board	
ADS131	1.818 mA
XLH736002	24 mA
TPS22860 (3)	6 nA
OPA4344 (2)	500 μA
ADXL354	200 μA
ADG734 (2)	40 nA
PDMS MCU	
Teensy 4.1	100 mA
Strain gauges	
120 Ω Concrete Gauges (3)	39 mA
Total	165.5 mA

Additionally, the theoretical cracking strain limit of a precast structure can be determined according to ACI 2011 [45] to identify the occurrence of cracks by using Eqs. (2)–(4):

$$f_r = 0.625\sqrt{fc'} \tag{2}$$

$$E_c = 4700\sqrt{fc'} \tag{3}$$

$$\varepsilon_{cr} = \frac{f_r}{E_c} \tag{4}$$

where *Ec*is the elastic modulus of concrete, and fc' is a concrete compressive strength based on concrete properties mentioned in Table 3. Depending on the property of the PCS, its cracking limit can be determined.

Step2: Sensor Installation & Monitoring

The second step in safety evaluation is careful installation of sensors on the PCS at the identified zero-strain locations. The three-channel strain gauges and the accelerometer were attached atop the PCS, and an accelerometer was installed at the center of the PCS to measure tilts from acceleration. The obtained raw data had initial offsets. In the safety assessment of PCS, absolute strain is the critical factor, and it is obtained using the offset adjustment method mentioned in step 3.

Step3: Strain Adjustment

To obtain absolute strain, the measured strains are adjusted relative to the strains in the lifting process, which are close to zero. After obtaining the absolute strain, the next step is to determine the maximum strain. To access safety, the maximum tensile strain at the top or bottom of the PCS should not exceed its cracking strain limit. The strains at the top were obtained from the measured data. However, gauge installation on the bottom surface of the PCS was not feasible. Therefore, the bottom strains were calculated indirectly with the aid of the FE model of the PCS. The details are provided in Section 4.4.

Step4: Safety Assessment

The obtained maximum strains were compared with the threshold value of 133 με, and strain limits of 75–100%, 50–74%, and 0–49% of the cracking strain were set as the high, medium, and low-risk levels in the safety evaluation process. The maximum tensile strains are highlighted in Fig. 10 and summarized in Table 4. The risk levels can be used as warning indicators in future works. The sensor will provide an alert if the measured strain exceeds the specified level; otherwise, it will continue to record measurements.

3. Application to on-site monitoring

3.1. Experimental setup

3.1.1. Description of PCS

An experiment that simulated the resting, lifting, and transportation of a PCS was conducted to validate the performance of the proposed PDMS and its safety assessment strategy. Notably, the proposed framework can be applied to other types of PCS such as, 9-m- and 5-m-long panels or precast girders. The PCS used in the experiment was a precast panel located at the Bricon R&BD plant in Chungbuk, South Korea. The PCS has a length of 12.14 m and the thickness of the PCS varies from 240 to 360 mm, which made it asymmetric, as illustrated in its front view in Fig. 4. A total of 20 shear pockets were present on PCS, but a few of the shear pockets were filled with concrete. Eight steel anchors were embedded on the top surface of PCS for attaching cables. The diameter of each cable was 22 mm. The cracking strain limit for of precast panel was 133 με, as determined using Eq. (4).

3.1.2. Sensor placement

The portable sensor, comprising a three-axis accelerometer and three channel strain gauges was deployed, and it recorded measurements in real-time at 100 Hz. The three-channel acceleration was measured to

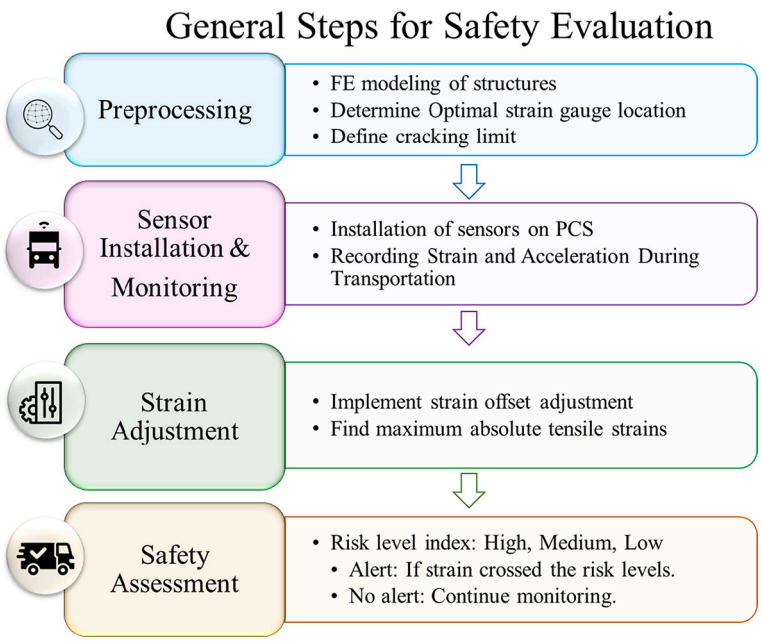

Fig. 3. Flowchart of safety evaluation.

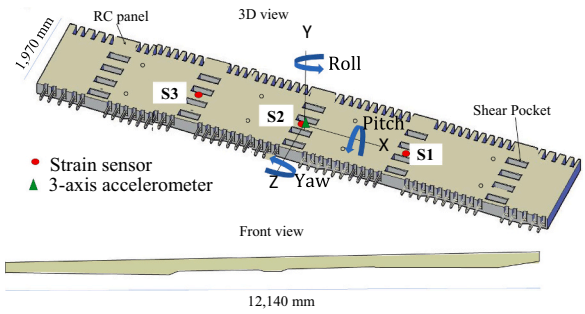

Fig. 4. PDMS assembly setup on PCS.

record the vibration and tilt of the PCS center, while the strain gauges were installed based on the results of an FE simulation of the lifting conditions by following step 1 in the safety assessment strategy. The final strain gauge installation locations S1, S2, and S3 were symmetric with respect to the PCS center, as depicted in Fig. 4, and the detailed process is discussed in Section 3.3.

3.1.3. PCS delivery stages

The PCS delivery process comprised four stages in the following sequence: the ground resting (GR) stage, in which the PCS was placed on five wooden supports in the yard; the airlifting (AL) stage, in which cables were attached to eight lifting points set on the upper surface of PCS, and the PCS was lifted using cranes; the truck resting (TR) stage, in which the PCS was placed on wooden supports on the bed of a truck, as shown in Fig. 5; and the transportation stage, in which truck started moving toward the installation site. Herein, we discuss these four stages, namely GR, AL, TR, and transportation.

3.1.4. PCS delivery timeline

The times corresponding to all PCS delivery stages were observed, and they are listed in Table 2. Initially, the PCS remained in the GR stage for 8 min. The lifting cables were hinged using the steel anchors embedded into the deck slab for lifting the PCS by using cranes. Approximately 14 min were required to load the PCS into the vehicle. The PCS delivery stage lasted almost 23 min, starting from minute 27 and ending at minute 50. After the transportation stage, the PCS remained on the truck for 25 min, after which it was lifted and laid back on the ground.

Table 2
Timeline of PCS delivery.

Sequence	Elapsed time (min)	Event/Stage
1	0–8	Ground Resting (GR)
2	8–14	Air Lifting (AL)
3	14–27	Truck Resting (TR)
–	–	Break
4	27–50	Transportation
5	50–75	Truck Resting (TR)
6	75–80	Air Lifting (AL)
7	80–85	Ground Resting (GR)

Fig. 5. a) PDMS positioned on the PCS in the GR stage, b) AL stage monitoring, and c) TR stage.

3.2. FE modeling and analysis of PCS

FE modeling and analysis was performed to find the optimal sensor location for safety assessment and validation purposes. This section describes the FE modeling of the reinforced PCS in the Abaqus software environment for simulating actual events [46].

The PCS was designed according to the provided 2D geometry with an unequal bottom surface slope. Three main models were generated: the first model corresponded to the airlifting stage (AL). The second model was of the GR condition with timber supports at the bottom of the reinforced PCS. The third model covered the TR stage with timber supports of varying sizes and numbers present at different locations compared to those in the GR stage. The material properties of concrete, steel, cables, and supports are presented in Table 3. The precast deck panel was modeled using as solid, C3D8R, 8-node linear brick elements, and the embedded reinforcement was modeled using T3D2, 2-node linear, and 3D truss elements measuring 16 mm in diameter [47]. The entire model was fine meshed with a 50-mm mesh control size. Contact control was assigned to the slabs and bars to prevent relative motion between surfaces. The PCS was allowed to deform in every direction in the lifting simulation. The T3D2 elements were used for designing the cables with a diameter of 22 mm. The analysis was performed as a static linear analysis within elastic limits.

3.3. Determination of strain measurement location

The FE model of the lifting process was generated before the field experiment to optimize the strain measurement locations. In total, eight cables were connected to the PCS by creating wire joints and setting connector sections as pin connections. Thereafter, meshing was performed, and FE analysis was conducted. The obtained strains were relatively close to zero. This reduction in the strain values during lifting was attributed to the balanced eight-point lifting scheme. The gauge positions were optimized such that the installation location of each gauge was close to a point of zero strain, and the symbols S1, S2, and S3 represent the strain gauges 1, 2, and 3, respectively, on PCS, as shown in Fig. 6.

The optimal strain gauge locations were selected as the points that exhibited almost zero strain during the lifting process, as shown in Fig. 6. The gauges and the accelerometer were installed at the selected locations. The field data were then processed by maintaining the strains close to zero at the locations of the three gauges in the lifting stage. The offsets of the field data for the GR and TR cases were adjusted.

Table 3
Assumed parameters of the FE model.

Parameter	*Value*	*Units*
Concrete		
Elastic modulus	27,000	MPa
Density	2.1×10^{-9}	tons/mm^3
Poisson's ratio	0.16	
Steel bars		
Elastic modulus	210,000	MPa
Density	7.8×10^{-9}	tons/mm^3
Poisson's ratio	0.3	
Cables		
Elastic modulus	170,000	MPa
Density	7.8×10^{-9}	tons/mm^3
Poisson's ratio	0.3	
Timber		
Elastic modulus	14,000	MPa
Density	6×10^{-9}	tons/mm^3
Poisson's ratio	0.18	

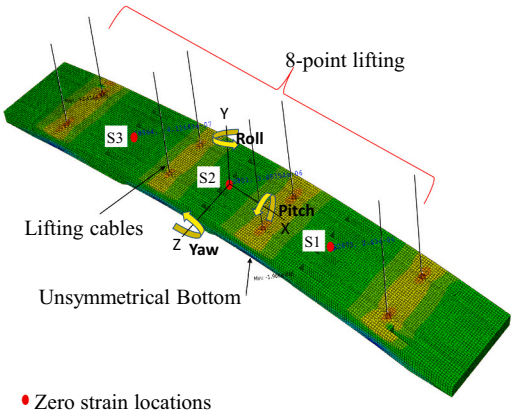

Fig. 6. Stress distribution of FE model during lifting.

4. Field observation

4.1. Acceleration measurement

Three-axis acceleration values were measured at 100 Hz continuously for 80 min throughout the delivery process, and a high-pass filter with a cut-off frequency of 0.1 Hz was applied to the acceleration data to compensate for offsets in the measurement, as depicted in Fig. 7.

The standard deviations of the vibrations along the *x*-, *y*-, and *z*-axes were 16.27 mg, 48.62 mg, and 23.65 mg, respectively, indicating that the vertical direction (i.e., y-axis) experienced the strongest vibration during transportation. The peak accelerations along the *x*-, *y*-, and *z*-axes were 164.89 mg, 682.59 mg, and 273.94 mg with durations shorter than 2 s. The peak vibrations did not reach the vertical (i.e., 1000 mg) and transverse (i.e., 500 mg) vibration limits specified in the general transport condition for road transport within the Cargo Transport Units (CTU) Code [48], and the structure was considered safe for vibration during transportation.

4.2. Tilt measurement

The three-axis raw acceleration measurement data were converted into the tilt of the structure by using Eqs. (5) and (6):

$$\theta_x = tan^{-1}\left[\frac{acc_x}{\sqrt{acc_y{}^2 + acc_z{}^2}}\right] \tag{5}$$

$$\theta_z = tan^{-1}\left[\frac{acc_z}{\sqrt{acc_x{}^2 + acc_y{}^2}}\right] \tag{6}$$

where acc_x, acc_y, and acc_z denote the accelerations along the *x*-, *y*-, and *z*-axes, respectively, and θ_x and θ_z denote pitch and yaw.

The pitch and yaw were close to 0 in the GR stage, but they increased suddenly to 2.1° and − 0.5°, respectively in AL stage (Fig. 8). The tilt did not change during the AL stage, indicating that the structure was well balanced and did not experience turnover and force transfer between cables. In the transportation stage, where the truck was on the road, the tilt fluctuated, but it was restored at the end of the transportation stage. This observation pertaining to tilt suggests that there was no significant change in the movement of the PCS

4.3. Raw strain measurement

Strains were measured at the three locations indicated in Fig. 4. The raw strain measurement was initialized at zero in GR stage, as displayed in Fig. 9. A comparison of the measured strains with the cracking limit of 133 με revealed that the strain recorded by S1 reached 95% of the limit

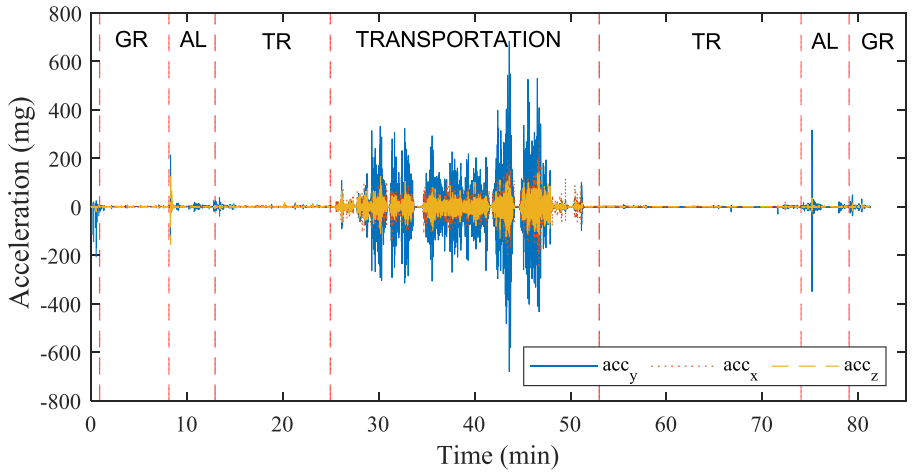

Fig. 7. Acceleration measured during experiment.

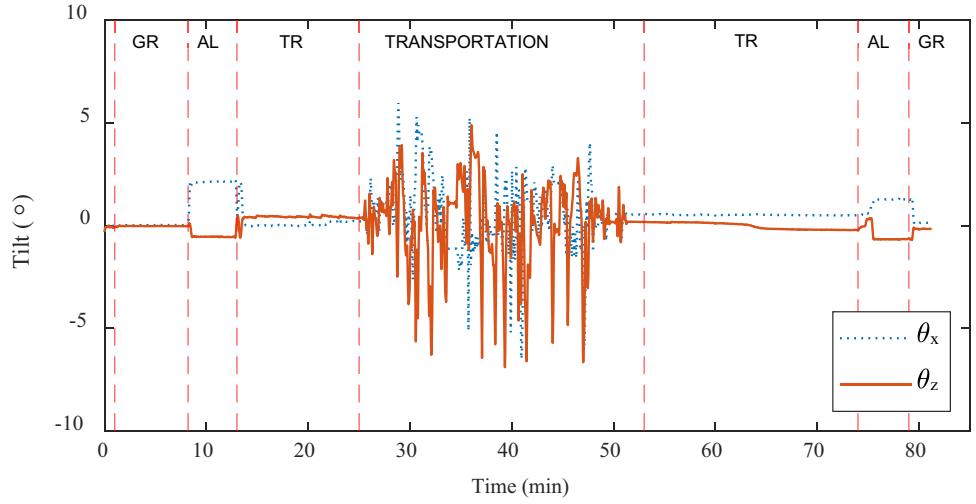

Fig. 8. Tilt measured during the experiment.

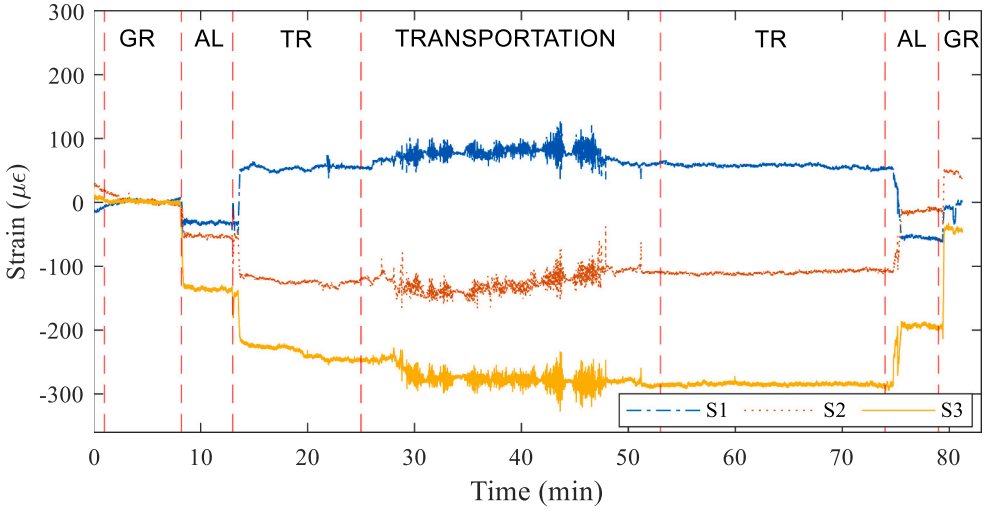

Fig. 9. Raw strain measurements obtained from S1, S2, and S3.

(i.e. 127 με) during transportation, but it did not exceed the limit. This indicated that the structure was in a high-risk condition without the presence of any crack.

4.4. Offset-adjusted strain measurement

Since the initial offset for strain cannot be measured unless the strain gauge is embedded in the structure during its manufacture, strain measurements cannot indicate the absolute stress distribution in the structure. Therefore, a proposed offset adjustment method is developed to determine the absolute strain by adjusting the strain measurements in the lifting stage that are close to zero. As described in Section 4.3, the sensors were installed at locations with zero strain, as obtained from the FE analysis, and strain measurements were processed by ensuring that the strains in the AL stage were close to zero. Before data processing, the strains in the GR stage were zero (Fig. 9), however, after offset adjustment, the maximum resulting tensile strain during the GR stage was 127 με at S3 (see Fig. 10a). It is worth noting that the value recorded by S3 after offset adjustment was quite close to the cracking limit, even in the GR stage, whereas raw strain measurements did not show any sign of damage in the GR stage.

In TR stage, the adjusted measurement indicated compressive strain at all three gauges, and the highest compressive value of 204 με was observed at S3. Because the strain gauges were attached onto the top surface of the PCS, strain applied on the bottom of the PCS was also investigated indirectly to find applied tensile strain at the bottom surface. The strains on the bottom surface were estimated by assuming a linear distribution of strain along the cross-section. First, the neutral axis along which stress becomes zero at the cross-section was obtained using the FE model. Next, the strain on the bottom surface was calculated using Eq. (7):

$$\varepsilon_b = \varepsilon_t \left(\frac{y}{h - y} \right) \tag{7}$$

where h is height of the cross-section, y is distance between the neutral axis and the top surface, (ε_b) and (ε_t) are strains on the bottom and top surface, respectively. The calculated strain on the bottom surface is depicted in Fig. 10b. According to the figure, the peak value of bottom strain at S3 is 195 με, which exceeds the cracking limit, while the strains at S1 and S2 are in the safe strain region. The safety of the PCS can be assessed by monitoring the top and bottom strains, and the PCS used in the experiment was found to be unsuitable for field application.

On the basis of the discussions in the above sections, the threshold value was calculated as 133 με, which was considered the cracking strain limit, according to ACI 2011 [45]. The cracking strain limit can serve as a warning indicator of PDMS for drivers during the transportation of PCS on trucks. Table 4 presents the results of a comparative condition assessment between the conventional method that uses raw strain measurement and the offset-adjusted strain measurement method proposed herein. In the case where raw strain measurements are used, the PCS is at a high risk of top strain and cracking on the bottom surface only in the transportation stage. By contrast, the offset-adjusted results indicate the high-risk condition of the structure in the GR stage and crack occurrence in the transportation stage.

Table 4
Condition assessment based on strain measurement.

	Strain without offset adjustment	Strain with offset adjustment (Top)	Strain with offset adjustment (Bottom)
Maximum Tensile Stress	127 με	127 με	195 με
Assessment	High-risk condition detected in transportation stage	High-risk condition detected in GR stage	High-risk condition detected in TR stage/ Crack occurrence detected in transportation stage

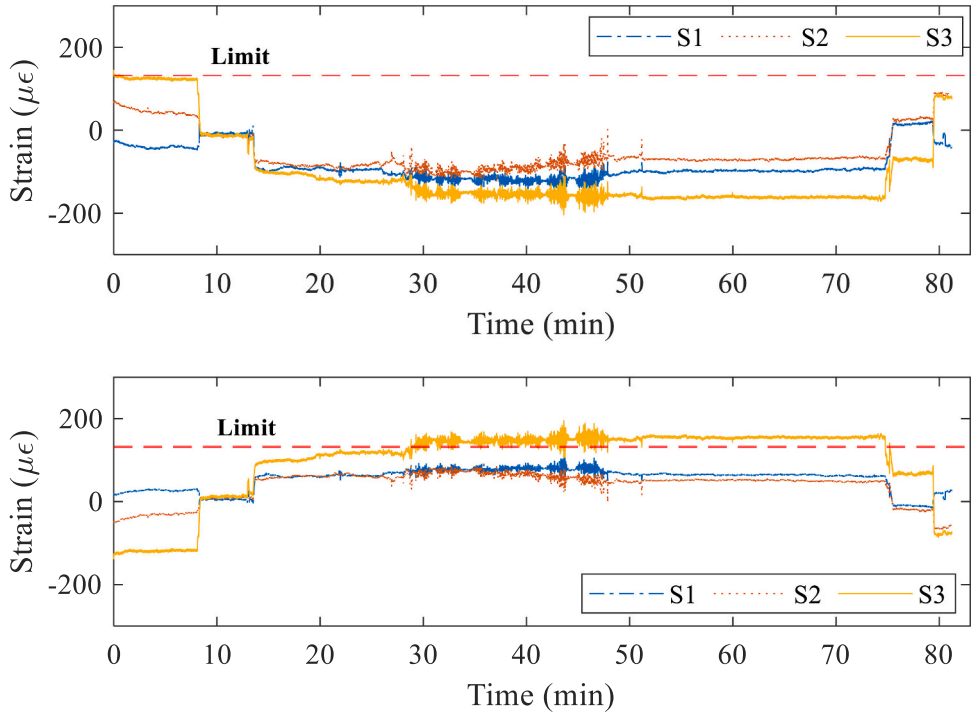

Fig. 10. a) Offset-adjusted strains on the top surface of the PCS, and b) calculated offset-adjusted strains on the bottom surface of the PCS.

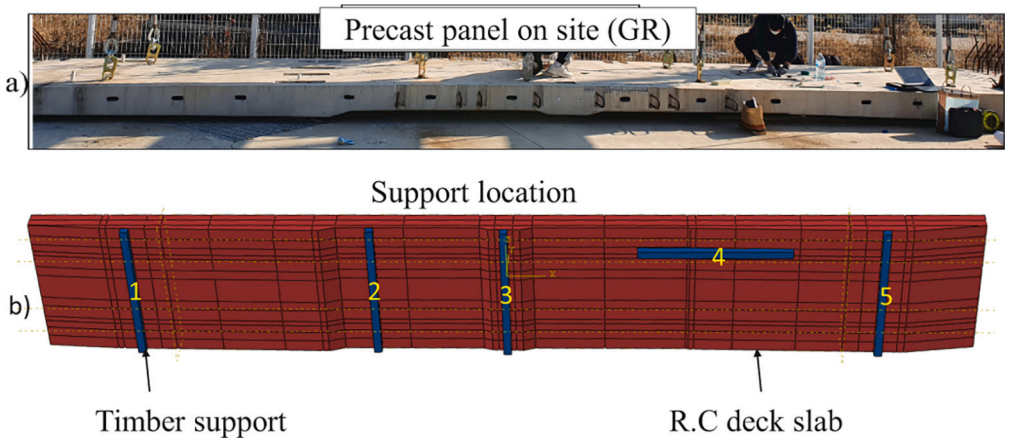

Fig. 11. a) Longitudinal profile of PCS in the GR stage, and b) FE model with five supports.

5. Discussion

5.1. Effect of support condition on strain distribution

The GR stage was modeled by placing the PCS over five supports (100 × 100 mm^2 area) under gravity loading as per on-site support conditions, depicted in Fig. 11. In the FE model, the connection between the supports and the slab was modeled by creating an interaction property. The bottom surfaces of the supports were fixed.

The initial strain offsets in the GR stage, as shown in Fig. 10, can be explained by examining the effects of different initial support displacements. In the GR stage, the uneven longitudinal profile of the PCS as well as the heights of different timber supports can cause an uneven stress distribution. Therefore, support optimization was performed to reduce the difference between the offset-adjusted strain measurement and the FE model by introducing an initial displacement at support no. 2 near the third strain gauge, as observed on site (Fig. 11b), to investigate the effect of support height and the corresponding strain distribution. The initial displacement of support no. 2 was increased from 0 to 20 mm in increments of 5 mm (Fig. 12). The model indicated uneven strain distribution in the PCS, tensile strain was observed at S3, and compressive strain was observed at S1 (Fig. 12). These results were similar to the distribution of offset-adjusted strain, as summarized in Table 5. Therefore, the FE model with the initial displacement of 10 mm was considered for comparison with the adjusted strain measurement, and it is displayed in Fig. 14a. This analysis suggested that even a minor change in the height of the support dramatically affects the strain distribution.

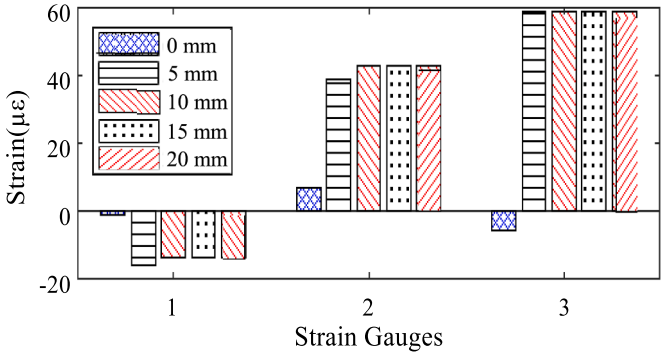

Fig. 12. Effect of changing initial displacement of timber support no. 2 from 0 to 20 mm.

5.2. Observations related to support condition in TR stage

The support condition in the TR stage was observed carefully. As depicted in Fig. 13a, to ensure safety, the workers placed seven supports under the structure evenly, but only three timber supports were in actual contact with structure, as indicated in the enlarged sections. This lack of contact at all points between the structure and the supports was ascribed to the asymmetrical shape of the structure. The site conditions were reflected in the FE modeling of the TR stage by considering only three supports (Fig. 13b). During modeling of TR stage, the optimal support condition was achieved by setting the initial displacement of the first and third supports to 5 mm (see Fig. 14b). The strain distribution obtained from the FE model deviated from the adjusted strain value measured using the PDMS owing to uncertainty in material, geometric properties, and support condition, Notably, S1, S2, and S3 were under compression, as monitored using the PDMS (see Table 5). The FE model with the updated boundary condition suggested that timer support no.1 and 3 were at higher positions than support no. 2, which induced compression on the top surface.

5.3. Considerations for support condition during delivery

The Support condition at GR and TR stage were investigated in Section 5.1, 5.2 and it was observed that strain distribution on the structure varies by not only the number of the supports but also contact condition of each support. In the GR stage, the position of the timber support no.2 was higher than other supports inducing tension at the left half of the structure. In the TR stage, the top strains were in compression due to relatively lower position of support no.2 compared with no.1 and no.3. Further, analysis was carried out using an FE model with an ideal support condition, in which five timber supports were spaced equally and were in full contact with the structure. The FE analysis was performed by first changing the support size and then determining the support position and number to achieve the minimum strains. It was observed that a minimum of five supports with a size of 100 mm placed at positions where the asymmetrical bottom has large gaps with ground surface can minimize the high strain values (Fig. 14c). The statistical mean of the monitored data was computed during each stage of delivery for comparison with the simulated data. The comparison results and the ideal strain values applied to the structure are summarized in Table 5. The resulting strains are in low-risk range, and their values do not exceed 50 με for both tension and compression, indicating the importance of contact condition and number of supports.

5.4. Practical considerations for field applications

The developed system is a novel contribution to the current practices

Table 5
Comparison of strain values of the FE model for different cases.

	Monitored Data			FEM			FEM		
				Considering Field Support Condition			Considering Ideal Field Support Condition		
	S1	S2	S3	S1	S2	S3	S1	S2	S3
GR stage	−40	58	139	−20	40	61	−21	24	−6.9
TR stage	−87	−75	−108	−76	−80	−61			

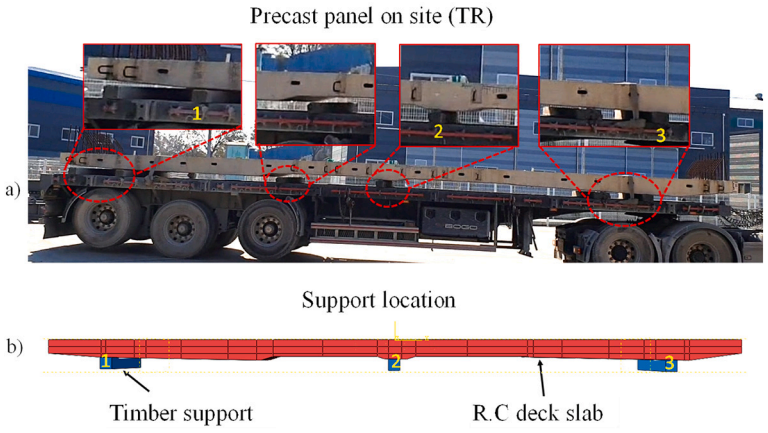

Fig. 13. a) Actual support condition in TR stage, and b) FE model with three supports.

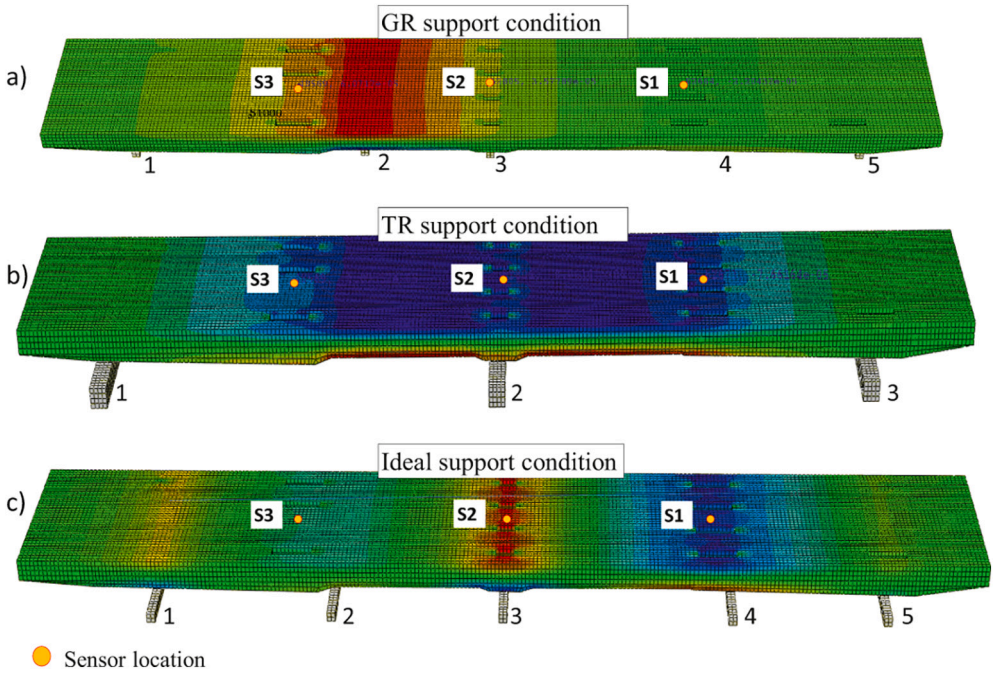

Fig. 14. a) Support condition in GR stage, b) Support condition in TR stage, c) Ideal field support conditions.

because thus far, hardly any research has been conducted to highlight the concept of absolute strain for PCS monitoring and safety by using a portable device. The proposed system can be useful for monitoring PCS, however, the following limitations should be considered in future studies to improve the applicability of the PDMS.

Need for FE model: An FE model is required to determine the optimal strain measurement position during the lifting process. Only boundary condition that FE model should consider is position for lifting cables, other than this, the monitoring system does not require generate models for the GR and TR stages with different support conditions. For simplified lifting analysis, a parametric model for a general type of structure can be considered.

Sensor installation: Sensors are fixed on the surface of concrete structures by drilling screws into them, which can damage the structures. In the field test, a thin steel plate was attached to a concrete surface with epoxy, and sensors with four magnets were mounted on the plate for recording measurements. This installation process can be simplified to a greater extent for practical implementation.

Online monitoring: Data processing after delivery of the structure may extend the workflow at the site. For practical implementation of the system, an online monitoring system that receives and processes data online by using cloud services is required.

6. Conclusions

This paper incorporates the successful development and implementation of a portable multimetric sensor system for assessing the condition of PCS during transportation. To this end, first, we developed a portable delivery monitoring system (PDMS) that supports a high sampling rate of 100 Hz for measuring both strain and acceleration continuously for up to four days during the transportation of PCS. In addition, a safety evaluation strategy was developed to assess the maximum strain on the structure by using offset-adjusted strain measurements.

With the developed system, a field experiment involving the actual transportation of a PCS was conducted. The PCS used herein was a 12-m-long precast concrete deck panel. The PCS was initially in the GR stage, and it experienced AL and transportation. The acceleration, tilt, and strain measurements of the PCS were analyzed to investigate its safety. In the AL stage, the tilt values obtained using the PDMS were stable, suggesting that the lifting process did not cause overturning or force distribution in the lifting cables. In the transportation stage, the proposed offset adjustment approach that adjusts the offsets of the measured raw strain data was applied, and the obtained offset-adjusted strains were compared to the cracking strain limit specified in ACI 2011 for safety assessment. The assessed data revealed that the structure was at a high-risk level in the GR stage, and a crack formed in the transportation stage because the structure was excited by the movement of the truck. Further investigation was conducted to explain the differences in strain distributions across the GR and TR stages, which were expected to have similar strain levels. The investigation revealed that the contact condition between the timber supports and the structure heavily affected the strain distribution. Therefore, evenly spaced and fully contacted supports, the so-called ideal support conditions, were suggested to considerably reduce the strain applied to the structure and ensure that it remains at a low risk level. Overall, the results indicate that the PDMS can serve as an efficient monitoring system for measuring acceleration and strain during PCS transportation, and crack occurrence can be identified through the proposed strain offset adjustment. Moreover, the support condition of the structure highly affects its strain distribution, thus highlighting the need for proper support deployment during transportation. Our results indicate the effectiveness of using the PDMS for precast monitoring, but they do not indicate that the system can support real-time data management for making timely decisions. Future work will seek to develop a cloud-based monitoring system that detects anomalies and alerts users to facilitate real-time decision-making for securing quality of precast structures during their transportation.

Declaration of Competing Interest

The authors declare that they have no known competing financial interests or personal relationships that could have appeared to influence the work reported in this paper.

Data availability

Data will be made available on request.

Acknowledgment

This research was conducted with the support of the “National R&D Project for Smart Construction Technology (No.22SMIP-A156887-02; No.22SMIP-A158708-03)” funded by the Korea Agency for Infrastructure Technology Advancement under the Ministry of Land, Infrastructure, and Transport and managed by the Korea Expressway Corporation and the Chung-Ang University Young Scientist Scholarship (CAYSS) grants in 2022.

References

[1] K.S. Elliott, Precast Concrete Structures, CRC Press, 2019, 100072588X.
[2] A. Nicał, H. Anysz, The quality management in precast concrete production and delivery processes supported by association analysis, Int. J. Environ. Sci. Technol. 17 (1) (2020) 577–590, https://doi.org/10.1007/s13762-019-02597-9.
[3] P.K. Priya, M. Neamitha, A review on precast concrete, Int. J. Eng. Technol. 5 (1) (2018) [Online]. Available at: https://www.irjet.net/archives/V5/i1/IRJET-V5I1204.pdf.
[4] D.K. Merritt, B.F. McCullough, N.H. Burns, Texas tests precast for speed and usability, J. Publ. Roads 66 (1) (2002) 30–34 [Online]. Available at: https://highways.dot.gov/public-roads/julyaugust-2002/texas-tests-precast-speed-and-usability.
[5] S.G. Joshi, Safety Risk Assessment and Improvement Method for Precast/Prestressed Concrete Industry Plant, Mississippi State University, 2021. Accessed: Sep 2021. [Online]. Available at: https://www.proquest.com/docview/2544935192?pq-origsite=gscholar&fromopenview=true.
[6] R. Cojocaru, Lifting analysis of precast prestressed concrete beams, Virginia Tech Master Thesis 21336, 2012. Accessed: Mar 2012. [Online]. Available at: http://hdl.handle.net/10919/32464.
[7] U.K. CROSS, Failure of Prestressed Hollowcore Units During Lifting (Report id: 749), Report. Accessed: Oct 2018. [Online]. Available at, https://www.cross-safety.org/uk/safety-information/cross-safety-report/failure-prestressed-hollowcore-units-during-lifting-749, 2018.
[8] T. Stratford, C.S. Burgoyne, Lateral stability of long precast concrete beam, Proc. Inst. Civ. Eng. Struct. Build. 134 (2) (1999) 169–180, https://doi.org/10.15554/pcij.01011989.34.53.
[9] S.D. Tayabji, Jointed precast concrete pavement panel fabrication and installation checklists, United States Federal Highway Admin. ID43533, 2019. Accessed: Jan 2019. [Online]. Available at: https://www.fhwa.dot.gov/pavement/pubs/hif19016.pdf.
[10] T. Stratford, C. Burgoyne, The toppling of hanging beams, Int. J. Solids Struct. 37 (26) (2000) 3569–3589, https://doi.org/10.1016/S0020-7683(99)00059-1.
[11] A. De la Fuente, J.M. Bairán, S.H.P. Cavalaro, Case study of failure of long prestressed precast concrete girder during lifting, Eng. Fail. Anal. 100 (2019) 512–519, https://doi.org/10.1016/j.engfailanal.2019.02.061.
[12] T. Wipf, B. Phares, J. Bigelow, T. Hosteng, A. Nadermann, Evaluation of the 24th Street Bridge, Institute for Transportation, Iowa State University, Ames, IA, 2010. Accessed: Nov 2010. [Online]. Available at: https://intrans.iastate.edu/app/uploads/2018/03/24th_st_bridge_w_cvr.pdf.
[13] C.P. Pantelides, J. Ries, R. Nix, Construction and monitoring of a single-span bridge with precast concrete glass-fiber-reinforced polymer reinforced deck panels, PCI J. 58 (1) (2013) 78–95, https://doi.org/10.15554/pcij.01012013.78.95.
[14] G. Laszlo, R.R. Imper, Handling and shipping of long span bridge beams, PCI J. 32 (6) (1987) 86–101, https://doi.org/10.15554/pcij.11011987.86.101.
[15] K.M. Holden, C.P. Pantelides, J.M. Ries, S.H. Malan, Lifting of GFRP precast concrete bridge deck panels, J. Perform. Constr. Facil. 29 (3) (2015), https://doi.org/10.1061/(ASCE)CF.1943-5509.0000563.
[16] S. Arabi, B. Shafei, B.M. Phares, Fatigue analysis of sign-support structures during transportation under road-induced excitations, Eng. Struct. 164 (2018) 305–315, https://doi.org/10.1016/j.engstruct.2018.02.031.
[17] Standards Australia, AS 2550.1–2011 Cranes, Hoists, and Winches—Safe Use General Requirements [Online]. Available at, https://infostore.saiglobal.com/en-au/standards/as-2550-1-2011-124169_saig_as_as_268272/, 2011.
[18] P.I. Cakmak, E. Tezel, A guide for risk management in construction projects: Present knowledge and future directions, in: Nthatisi Khatleli (Ed.), Risk Management in Construction Projects, IntechOpen, 2019, https://doi.org/10.5772/intechopen.84361 [Online].
[19] H. Kennedy, K. Kennedy, Moving the Mars Stone Chapel–Pulaski, Tennessee, Struct. Movers 21 (2) (2003) 10–11.
[20] D. Telem, A. Shapira, Y.D. Goren, C.J. Schexnayder, Moving a reinforced-concrete building: case study, J. Constr. Eng. Manag. 132 (2) (2006) 115–124, https://doi.org/10.1061/(ASCE)0733-9364(2006)132:2(115).
[21] Z. Mi, L. Pan, J. Chen, L. Chen, R. Wu, Consecutive lifting and lowering electrohydraulic system for large size and heavy structure, Autom. Constr. 30 (2013) 1–8, https://doi.org/10.1016/j.autcon.2012.10.008.
[22] K. Li, J. Chen, Z. Xiao, M. Xu, An electrohydraulic system for synchronized roof erection, Autom. Constr. 12 (1) (2003) 29–42, https://doi.org/10.1016/S0926-5805(02)00038-9.
[23] T. Guo, E. Wu, A. Li, L. Wei, X. Li, Integral lifting and seismic isolation retrofit of great hall of Nanjing museum, J. Perform. Constr. Facil. 26 (5) (2012) 558–566, https://doi.org/10.1061/(ASCE)CF.1943-5509.0000273.
[24] C. Ciesielski, ADCIC-Automatic data collection in construction, in: Proceedings of AIM'S Global Academic and Scientific Conference, 2000.
[25] N. Murray, T. Fernando, G. Aouad, A virtual environment for the design and simulated construction of prefabricated buildings, Virtual Reality 6 (4) (2003) 244–256, https://doi.org/10.1007/s10055-003-0107-8.
[26] J. Neelamkavil, Automation in the prefab and modular construction industry, in: 26th Symposium on Construction Robotics ISARC, 2009, https://doi.org/10.22260/ISARC2009/0018.

[27] J. Goggins, S. Newell, D. King, M. Hajdukiewicz, Real-time monitoring of a hybrid precast and in-situ concrete flat slab system, J. Struct. Integr. Mainten. 37 (1) (2016) 303–320 [Online]. Available at: https://www.semanticscholar.org/paper/Real-time-monitoring-of-a-hybrid-precast-and-in-Goggins-Newell/a6ac0b51d8eb482950f910a1e60283d85a720ec2.

[28] C. Zhou, X. Li, J. Sun, B. Xie, Y. Wu, Lift monitoring and analysis of multi-storey corridors in buildings, Autom. Constr. 106 (2019), 102902, https://doi.org/10.1016/j.autcon.2019.102902.

[29] M. Abdulkarem, K. Samsudin, F.Z. Rokhani, M.F.A. Rasid, Wireless sensor network for structural health monitoring: a contemporary review of technologies, challenges, and future direction, Struct. Health Monit. 19 (3) (2020) 693–735, https://doi.org/10.1177/1475921719854528.

[30] J.A. Rice, et al., Flexible smart sensor framework for autonomous structural health monitoring, Smart Struct. Syst. 6 (5_6) (2010) 423–438, https://doi.org/10.12989/sss.2010.6.5_6.423.

[31] B.F. Spencer Jr., H. Jo, K.A. Mechitov, J. Li, S.-H. Sim, R.E. Kim, S. Cho, L. E. Linderman, P. Moinzadeh, R.K. Giles, G. Agha, Recent advances in wireless smart sensors for multi-scale monitoring and control of civil infrastructure, J. Civ. Struct. Heal. Monit. 6 (1) (2016) 17–41, https://doi.org/10.1007/s13349-015-0111-1.

[32] K. Shafique, B.A. Khawaja, F. Sabir, S. Qazi, M. Mustaqim, Internet of Things (IoT) for next-generation smart systems: A review of current challenges, future trends and prospects for emerging 5g-IoT scenarios, in: Institute of Electrical and Electronics Engineers (IEEE) Access 8, 2020, pp. 23022–23040, https://doi.org/10.1109/ACCESS.2020.2970118.

[33] Libelium, Waspmote v15 Datasheet [Online]. Available at, http://www.libelium.com/downloads/documentation/waspmote_datasheet.pdf (Accessed 08 July 2022).

[34] D.P. Hoover, A. Bilbao, J.A. Rice, Wisemote: a novel high fidelity wireless sensor network for structural health monitoring, Smart Struct. Syst. 10 (3) (2012) 271–298, https://doi.org/10.12989/sss.2012.10.3.271.

[35] R.A. Swartz, D. Jung, J.P. Lynch, Y. Wang, D. Shi, M.P. Flynn, Design of a wireless sensor for scalable distributed in-network computation in a structural health monitoring system, in: Proceedings of the 5th International Workshop on Structural Health Monitoring, 2005, pp. 12–14.

[36] B. Spencer Jr., J.-W. Park, K. Mechitov, H. Jo, G. Agha, Next generation wireless smart sensors toward sustainable civil infrastructure, Proc. Eng. 171 (2017) 5–13, https://doi.org/10.1016/j.proeng.2017.01.304.

[37] Y. Fu, K. Mechitov, T. Hoang, J.R. Kim, D.H. Lee, B.F. Spencer Jr., Development and full-scale validation of high-fidelity data acquisition on a next-generation wireless smart sensor platform, Adv. Struct. Eng. 22 (16) (2019) 3512–3533, https://doi.org/10.1177/1369433219866093.

[38] H. Jo, J.A. Rice, B.F. Spencer Jr., T. Nagayama, Development of high-sensitivity accelerometer board for structural health monitoring, in: Sensors and Smart Structures Technologies for Civil, Mechanical, and Aerospace Systems 2010 vol. 7647, International Society for Optics and Photonics, 2010, p. 764706, https://doi.org/10.1117/12.848905.

[39] M.Z. Sarwar, M.R. Saleem, J.-W. Park, D.-S. Moon, D.J. Kim, Multimetric event-driven system for long-term wireless sensor operation for SHM applications, Inst. Electric. Electron Eng. (IEEE) Sensors J. 20 (10) (2020) 5350–5359, https://doi.org/10.1109/JSEN.2020.2970710.

[40] S.-H. Sim, B. Spencer Jr., T. Nagayama, Multimetric sensing for structural damage detection, J. Eng. Mech. 137 (1) (2011) 22–30, https://doi.org/10.1061/(ASCE)EM.1943-7889.0000199.

[41] A. Kumar, I.P. Singh, S.K. Sud, Development of multi-channel data logger for indoor environment, Eng. Fail. Anal. 2 (09) (2010) 690, https://doi.org/10.4236/eng.2010.29089.

[42] J. Won, J.-W. Park, J. Park, J. Shin, M. Park, Development of a reference-free indirect bridge displacement sensing system, Sensors (2021), https://doi.org/10.3390/s21165647.

[43] W. Greiman, Arduino sdfat Library [Online]. Available at, https://www.if.ufrj.br/~pef/producao_academica/artigos/audiotermometro/audiotermometro-I/bibliotecas/SdFat/Doc/html/.

[44] M.U. Hashmi, W. Labidi, A. Bušić, S.-E. Elayoubi, T. Chahed, Long-term revenue estimation for battery performing arbitrage and ancillary services, in: 2018 Institute of Electrical and Electronics Engineers (IEEE) International Conference on Communications, Control, and Computing Technologies for Smart Grids (SmartGridComm), IEEE, 2018, pp. 1–7, https://doi.org/10.1109/SmartGridComm.2018.8587562.

[45] Building Code Requirements for Structural Concrete and Commentary, A. C. Institute (ACI), 2011 [Online]. Available at, https://www.concrete.org/store/productdetail.aspx?ItemID=318U11&Language=English.

[46] M. Smith, ABAQUS/CAE, Version 2020, Dassault Systèmes Simulia Corp, Providence, RI, 2020.

[47] Abaqus/Standard User's Manual, Version 2020, Dassault Syst{\`e}mes Simulia Corp, 2020 [Online]. Available at, https://www.3ds.com/support/hardware-and-software/simulia-system-information/abaqus-2020/.

[48] Code of Practice for Packing of Cargo Transport Units (CTU Code), IMO/ILO/UNECE, 2014 [Online]. Available at, http://www.unece.org/trans/wp24/guidelinespackingctus/intro.html.